JOURNAL OF NEUROTRAUMA 36:485–499 (February 1, 2019)

DOI: 10.1089/neu.2018.5713

Longitudinal Optogenetic Motor Mapping Revealed Structural and Functional Impairments and Enhanced Corticorubral Projection after Contusive Spinal Cord Injury in Mice

Jun Qian,[1,2] Wei Wu,[1] Wenhui Xiong,[1] Zhi Chai,[3] Xiao-Ming Xu,[1] and Xiaoming Jin[1]

Abstract

Current evaluation of impairment and repair after spinal cord injury (SCI) is largely dependent on behavioral assessment and histological analysis of injured tissue and pathways. Here, we evaluated whether transcranial optogenetic mapping of motor cortex could reflect longitudinal structural and functional damage and recovery after SCI. In Thy1-Channelrhodopsin2 transgenic mice, repeated motor mappings were made by recording optogenetically evoked electromyograms (EMGs) of a hindlimb at baseline and 1 day and 2, 4, and 6 weeks after mild, moderate, and severe spinal cord contusion. Injuries caused initial decreases in EMG amplitude, losses of motor map, and subsequent partial recoveries, all of which corresponded to injury severity. Reductions in map size were positively correlated with motor performance, as measured by Basso Mouse Scale, rota-rod, and grid walk tests, at different time points, as well as with lesion area at spinal cord epicenter at 6 weeks post-SCI. Retrograde tracing with Fluoro-Gold showed decreased numbers of cortico- and rubrospinal neurons, with the latter being negatively correlated with motor map size. Combined retro- and anterograde tracing and immunostaining revealed more neurons activated in red nucleus by cortical stimulation and enhanced corticorubral axons and synapses in red nucleus after SCI. Electrophysiological recordings showed lower threshold and higher amplitude of corticorubral synaptic response after SCI. We conclude that transcranial optogenetic motor mapping is sensitive and efficient for longitudinal evaluation of impairment and plasticity of SCI, and that spinal cord contusion induces stronger anatomical and functional corticorubral connection that may contribute to spontaneous recovery of motor function.

Keywords: corticorubral pathway; corticospinal tract; motor mapping; optogenetics; spinal cord injury

Introduction

Although the mature central nervous system (CNS) has a poor intrinsic capability of regeneration after injury, partial spontaneous functional recovery does occur after spinal cord injury (SCI).[1,2] Plasticity and reorganization of the CNS has been considered to underlie such functional recovery after SCI by generating novel neural circuits,[3–5] which involves mechanisms including axonal sprouting, synaptic plasticity, and neurogenesis.[6–10] These processes occur not only in spinal cord, but also in the cerebral cortex and subcortical structures such as the red nucleus and brainstem nuclei.[11,12]

However, current assessments of structural and functional impairments after SCI are largely dependent on tissue histology, track tracing, and behavioral assessment, making it difficult to correlate dynamic functional recovery with circuit plasticity. Although recordings of cortical motor evoked potentials and motor mapping provide an electrophysiological evaluation of injured motor pathways,[13,14] the invasiveness and inefficiency of conventional electrical stimulation and low spatial resolution of transcranial magnetic stimulation greatly limit their application for SCI study. Optogenetic mapping of motor cortex may provide a solution to this challenge. In Thy1-ChR2-YFP transgenic mice that express channelrhodopsin-2 (ChR2) mainly in layer 5 pyramidal neurons,[15,16] transcranial optogenetic stimulation can be used to activate ChR2-expressing neurons for mapping motor cortex.[17–20] Although this technique provides advantages, including non-invasiveness, cellular specificity, and good spatial and temporal resolution,[19,20] whether it is reliable and sensitive in reflecting damage and repair after contusive SCI has not been specifically characterized.

[1]Department of Anatomy and Cell Biology & Department of Neurological Surgery, Spinal Cord and Brain Injury Research Group, Stark Neuroscience Research Institute, Indiana University School of Medicine, Indianapolis, Indiana.
[2]Department of Spinal Surgery and Orthopedics, The First Affiliated Hospital of Anhui Medical University, Hefei, China.
[3]Research Center of Neurobiology, Shanxi University of Traditional Chinese Medicine, Taiyuan, China.

Corticospinal tract (CST) and corticorubrospinal pathway both connect motor cortex and spinal cord and function in controlling skilled voluntary movements of limbs.[21–23] Because of their respective dorsa-medial and lateral locations of the CST and rubrospinal tract (RST) in rodents, the CST is often severely damaged[24] whereas the RST is often partially or completely spared after spinal cord contusion. Such pathway specific damage and preservation provide a unique opportunity for studying the plasticity and reorganization of the corticorubrospinal tract after SCI. A recent study demonstrated spontaneous recovery of motor function after bilateral pyramidotomy, accompanied by extensive sprouting of intact rubrofugal and -spinal projections and formation of a new circuit between red nucleus and nucleus raphe magnu.[5] Promoting axonal sprouting by neutralizing myelin-associated neurite growth inhibitor restored skilled motor function of the forelimb, which was paralleled by corticorubral and -pontine fiber sprouting.[25] However, whether SCI causes reorganization of the corticorubral pathway, particularly in a contusive SCI model, has not been directly demonstrated.

Thus, the current study has two purposes. One was to determine whether optogenetic motor mapping could provide an efficient and sensitive approach for longitudinal evaluation of SCI and its plasticity in a clinically relevant contusive SCI model. The other was to use this technique to test whether SCI would cause reorganization of the CST and corticorubral pathway. In Thy1-ChR2-YFP transgenic mice that received graded SCI, we made repeated optogenetic motor mapping for up to 6 weeks to determine initial loss and subsequent recovery of motor map and the correlations between the motor map size and motor behavioral performance, spinal cord lesion area, or preservation of corticospinal and rubrospinal pathways. Together with retro- and anterograde tracings and immunostaining, we showed that longitudinal optogenetic motor mapping reflected not only injury severity, but also dynamic motor functional recovery after contusive SCI. We also found that SCI caused significant enhancement of the corticorubral, but not corticospinal, projection in this model.

Methods

Animals

A total of 52 female Thy1-Channelrhodopsin 2-YFP (ChR-2) transgenic mice (line 18, stock 007612, strain B6.Cg-Tg(Thy1-COP4/EYFP)18Gfng/J; The Jackson Laboratory, Bar Harbor, ME), 8–10 weeks of age and weighing 20–22 g, were used in this study. All animals were maintained in a 12/12-h light/dark cycle with food and water freely available. Surgical interventions, treatments, and post-operative animal care were performed in accord with Guidelines of the Institutional Animal Care and Use Committee of the Indiana University School of Medicine (Indianapolis, IN).

To determine whether optogenetic motor mapping could be used as a physiological measurement of functional deficits after SCI, we assigned 8 mice to each of a sham group and three SCI groups that received mild, moderate, and severe SCI respectively. All these animals received behavioral tests, optogenetic motor mapping, and retrograde tracing with Fluoro-Gold (FG). To determine motor pathway plasticity after SCI, 10 mice were divided into a sham group and a moderate SCI group. For each animal, anterograde tracing with biotin dextran amine (BDA) and retrograde tracing with FG were performed. To further determine plasticity of corticorubral projection after SCI, 10 mice were assigned to a sham group and a moderate SCI group for optogenetic stimulation of the motor cortex followed by c-Fos staining and synapse immunostaining.

Contusive spinal cord injury surgery

The SCI procedure was performed as described by Liu and colleagues.[26] Under anesthesia with ketamine-xylazine (87.7 mg/kg of ketamine, 12.3 mg/kg of xylazine), contusive SCI models were created at the T10 level using an Infinite Horizon Impactor (Infinite Horizons [IH], Lexington, KY). Three different impact forces (30, 60, and 90 kDyn) were used to create mild, moderate, and severe injuries, respectively. Mice in the sham groups underwent laminectomy, but without receiving an impact. After the laminectomy and SCI, the muscle and skin were closed in layers, and all animals were placed in a temperature- and humidity-controlled chamber overnight. Manual bladder expression was carried out twice-daily until reflex bladder emptying was established.

Behavioral assessments

Basso Mouse Scale (BMS) locomotor test, rota-rod, and grid walk test were performed. Every animal was trained for 1 week before surgery and all behavior tests were performed by experienced observers who were blind to the experimental groups. The BMS locomotor tests were performed at baseline and weekly up to 6 weeks after SCI according to a method published previously.[27] Briefly, the animal was placed in an open field (42 inches in diameter) and observed for 4 min by two observers. The score was on a scale of 0–9, which was based on hindlimb movements made in an open field including hindlimb joint movement, weight support, plantar stepping, coordination, paw position, and trunk and tail location.[26]

The rota-rod test was performed as published previously[28] at baseline and 2, 4, and 6 weeks after injury. Retention time of an animal staying on a rotating rod was measured at a rotation speed of 18 rpm using a five-lane rota-rod device (IITC Life Science, Inc., Woodland Hills, CA). The device was accelerated from 1 to 18 rpm over 90 sec, with each trial lasting a maximum of 120 sec. Trials ended when the animal either fell off the rod or clung to the rod as it made one complete rotation. Three trials were performed for each mouse at each test, and an average retention time was taken from the three trials.

The grid walk was also used to evaluate hindlimb locomotor deficits[29] and was performed at baseline and 2, 4, and 6 weeks after injury. Animals walked on a plastic mesh (1.5×1.5 square foot) containing 1.2×1.2 cm diamond holes. During the test, total hindlimb footfalls of each animal were counted by two observers blind to the experimental groups. The number of footfalls (fall of the hindlimb, including at least the ankle joint, through the grid surface) was determined individually for each hindlimb.[30]

In vivo *optogenetic motor mapping*

In vivo transcranial optogenetic motor mappings were made at baseline, 1 day, and 2, 4, and 6 weeks after SCI. Before baseline mapping, the skin above the bilateral motor cortex was removed, the skull was exposed and covered with a thin layer of cyanoacrylate glue, and the bregma was marked for reference (Fig. 1). For optogenetic mapping, each animal was anesthetized with ketamine-xylazine (80 mg/kg of ketamine, 4 mg/kg of xylazine, intraperitoneally [i.p.]) and placed on a platform. When a mouse responded to a tail pinch with a slight tail move, depth of anesthesia was regarded as appropriate for mapping.

We made motor cortical mapping by using a blue laser to stimulate the left motor cortex and recording an evoked electromyogram (EMG) of the contralateral hindlimb in each animal. Six stimulation regions were set in the left cortex, with two regions anterior to bregma and four regions posterior to bregma. There were 5×6 stimulation spots in each stimulation region and a total of 180 stimulation spots on the left cortex, which completely covered the hindlimb area of the left motor cortex. We used a laser scanning photostimulation system for optogenetic mapping.[31,32] A blue laser

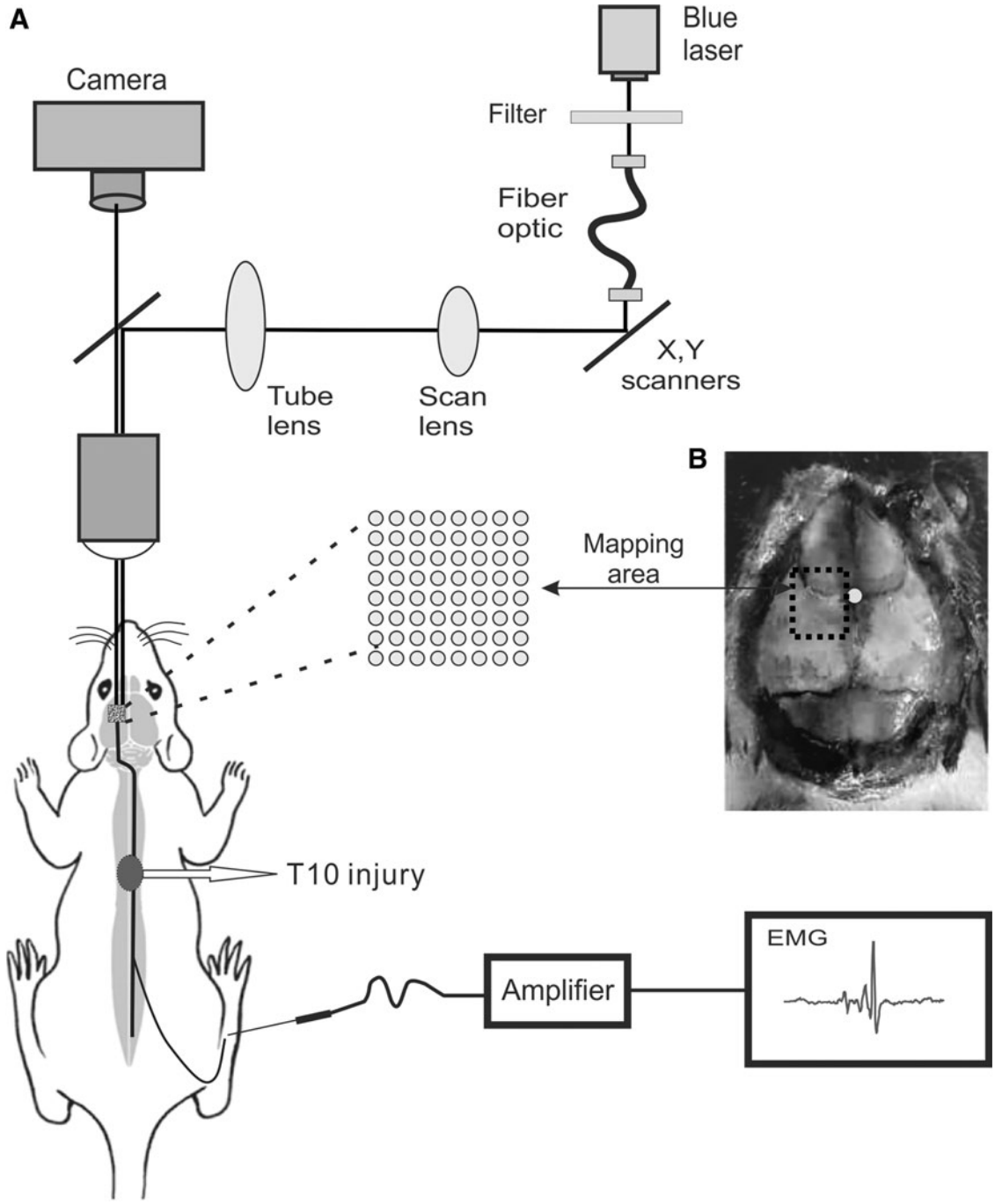

FIG. 1. A laser scanning photostimulation setup for optogenetic mapping of motor cortex in Thy1-ChR2 transgenic mice. (**A**) A mouse was anesthetized and the left motor cortex was photostimulated by a blue laser (470 nm) through a 5× microscope objective, and the evoked motor response was detected by an electrode inserted in the gastrocnemius muscle of the right hindlimb. (**B**) Six stimulation regions were set in the left motor cortex, with two regions anterior and four regions posterior to bregma. There were 30 stimulation spots in each region and totally 180 stimulation spots on the left cortex. The white dot in (B) indicates the location of bregma, and the black dashed area indicates the area of optogenetic mapping. EMG, electromyogram.

(470 nm) went through an optic fiber and a lens assembly that focused the light onto a dichroic mirror, which reflected the light beam to the back aperture of a 5× objective (Fluar 5×; Carl Zeiss, Jena, Germany) of an upright Olympus microscope and projected to the left cortex (Fig. 1A). In each mapping region, the blue laser scanned three times repeatedly. Upon finishing mapping one region, the next region was mapped by moving the microscopic field. A complete map was obtained by averaging the results from three maps at each region and combining the maps of the six regions together. Intensity of the blue laser was 17 mW at the maximum and could be attenuated through a neutral density filter. A pulse duration of 5 ms was used for motor mapping. EMG responses induced by optogenetic stimulation were recorded from gastrocnemius muscle of the contralateral hindlimb using two stainless steel needles. Responses were amplified, digitized, and recorded in a computer.

Events that occurred within 50 ms after laser flashes were detected using an event-detecting software. At each mapping spot, peak amplitudes of the event from three repetitions were averaged for comparison and map construction. In each motor map, different color spots represented different EMG amplitudes, with red spots having the higher amplitude and blue spots having the lower amplitudes (Fig. 2A). Total number of spots with positive EMG was counted to reflect the size of a cortical motor map. Average EMG amplitudes with respect to anterior-to-posterior or medial-to-lateral direction were calculated by dividing total EMG amplitudes along each column by total number of stimulating spots. Motor maps were constructed with OriginPro software (version 9.1; OriginLab, Northampton, MA).

Retrograde and anterograde tracings

After the final motor mapping and behavior tests, FG solution was injected into the spinal cord for retrogradely labeling spinal cord projecting neurons of the cortex and subcortical nuclei, using a previously described technique.[33] Before injection, laminectomy of the T12 vertebra was performed to expose spinal dura mater. A glass pipette attached to a Hamilton syringe was inserted into the spinal cord (0.3 mm from the midline, 0.5 mm from the dorsal surface of the spinal cord, and 10 mm caudal to the injury site) to inject 2% FG (Fluorochrome, Inc, Denver, CO). Every animal received two stereotaxic injections of 0.5 μL of FG each. The glass pipette was left in place for 5 min before moving to the next injection site. Mice were perfused for histological processing 1 week after FG injection. For simultaneous antero- and retrograde tracing, all animals received an FG injection, as described above, 1 week after BDA injection.

At 4 weeks post-SCI, 10 mice received a stereotaxic injection of BDA (10%; Molecular Probes, Eugene, OR) for tracing axons of the primary motor cortex. The protocol of BDA injection was described previously.[34] A 3×2 mm cranial window was made above the left motor cortex with a micro-drill to expose the dura mater. Five injections of 3 μL each were made at a rate of 0.15 μL/min and 0.6 mm deep into the cortex. Injection coordinates were as follows: 1.5 mm lateral and 2.0, 1.25, and 0.5 mm anterior to bregma; 1.0 mm lateral and 0.25 and 1.0 mm caudal to bregma. The BDA injection was made using the same system as the FG injection. The glass pipette was left in place for 5 min before moving to the next injection site.

Optogenetic stimulation of the motor cortex

To determine whether stimulating motor cortex would cause enhanced activation of cortical or subcortical neurons after SCI, 5 mice each were assigned to a sham group and a moderate SCI group. At 6 weeks post-surgery, a blue light-emitting diode (LED; 470 nm) was implanted on the left skull (1.5 mm lateral and 1.2 mm anterior to bregma) to stimulate the motor cortex. The LED was controlled by a miniature circuit that generated a burst of three pulses at 33 Hz once every 3 sec. After receiving 30 min of the optogenetic stimulation, mice were perfused and processed for immunostaining with c-Fos.

Tissue histology and immunofluorescence staining

Animals were deeply anesthetized with sodium pentobarbital (150 mg/mL) and transcardially perfused with 0.01 M phosphate-buffered saline (PBS) followed by 4% paraformaldehyde (PFA) in 0.01 M of PBS. Brain and spinal cord were dissected, post-fixed with 4% PFA overnight at 4 °C, and then transferred to 30% sucrose for 3–7 days. The brain was frozen within optimal cutting temperature in compound embedding matrix (SouthernBiotech, Birmingham, AL). Brain tissue containing cortex and red nucleus was sectioned coronally at 30-μm thickness on a cryostat set. Coronal sections were examined to evaluate neurons labeled by FG in the motor cortex and red nucleus. Immunofluorescence staining was performed to assess activated neurons labeled by c-Fos in the cortex and red nucleus, and BDA-labeled axons and FG-labeled neurons in the red nucleus.

For c-Fos fluorescence staining, brain sections were permeabilized with 0.1% Triton X-100 in PBS (0.1 M, pH 7.4), immunoblocked with 20% normal goat serum in PBS at room temperature for 1 h, and then incubated with a primary antibody against c-Fos (rabbit, 1:800; Sigma-Aldrich, St. Louis, MO) at 4°C overnight. Sections were then incubated with a goat antirabbit secondary antibody (1:200; Invitrogen, Carlsbad, CA) for 2 h at room temperature. For nuclear staining, 4',6-diamidino-2-phenylindole (DAPI; 1:10,000) was added to the final wash for 5 min. To visualize BDA-labeled axons, brain sections were incubated sequentially with ABC reagent (1:250, 30 min; Vector Laboratories, Burlingame, CA), biotinyl tyramide (1:75, 10 min; PerkinElmer Life Sciences, Waltham, MAQ), and extra-avidin fluorescein isothiocyanate (1:500, 2 h; Sigma-Aldrich). After BDA staining, the same sections were incubated with a primary antibody against synaptophysin (rabbit, 1:200; Abcam, Cambridge, MA) at 4°C overnight and then incubated with a goat antirabbit secondary antibody (1:200; Invitrogen) for 2 h at room temperature.

For histological assessments of SCI, all animals that had undergone optogenetic mapping at 8 weeks after SCI were sacrificed and perfused. Spinal cords containing the lesion epicenters were dissected out, embedded, and sectioned at 30 μm. A set of serial cross-sections of spinal cord were stained with cresyl violet and eosin. Lesion areas were outlined and quantified under an Olympus BX60 microscope equipped with a Neurolucida system (MicroBrightField, Colchester, VT) and ImageJ software (NIH, Bethesda, MD).

Quantification of biotin dextran amine–labeled axons, Fluoro-Gold–labeled neurons, and synapses

For quantification of neurons labeled by FG in the motor cortex and red nucleus, every third brain section involving anatomical sites of motor cortex and red nucleus were chosen. Only labeled cells that were fluorescent with clearly defined somata were counted. Boundaries of the motor cortex and red nucleus were established using a stereotaxic mouse brain atlas.[35] Using similar methods, the numbers of neurons co-labeled with c-Fos and DAPI were counted in every third brain section involving red nucleus. The number of labeled cells per section for each mouse was calculated by dividing the total number of labeled cells counted in that mouse by the number of counted sections that contained the motor cortex or red nucleus.

To quantify the BDA-labeling axons projecting from the motor cortex to red nucleus, serial brain sections involving the red nucleus were chosen. Density of BDA labeled axons was quantified using NIH ImageJ software as described previously.[10] Under low magnification ($10\times$objective), the outline of red nucleus was drawn, BDA-labeled axons within the red nucleus were detected, and then density of BDA-labeled axons was quantified. The number of synapses was counted using a method described previously.[36] Spots of co-localization between BDA-labeled axons and FG-positive neurons in each counting area under high magnification ($40\times$objective) were counted and corrected by the number of FG neurons in the same area within the red nucleus. In each animal, we chose three sections for quantifying the density of BDA-labeled axons and the number of synapses, respectively.

Recording corticorubral synaptic responses in vivo

Ten C57Bl mice, at 2.5–3.0 months old, were equally assigned to a sham group and a moderate SCI group. At 6 weeks after SCI or sham surgery, mice were anesthetized with i.p. injection of 250–500 mg/kg of Avertin. After a mouse was placed on a stereotactic

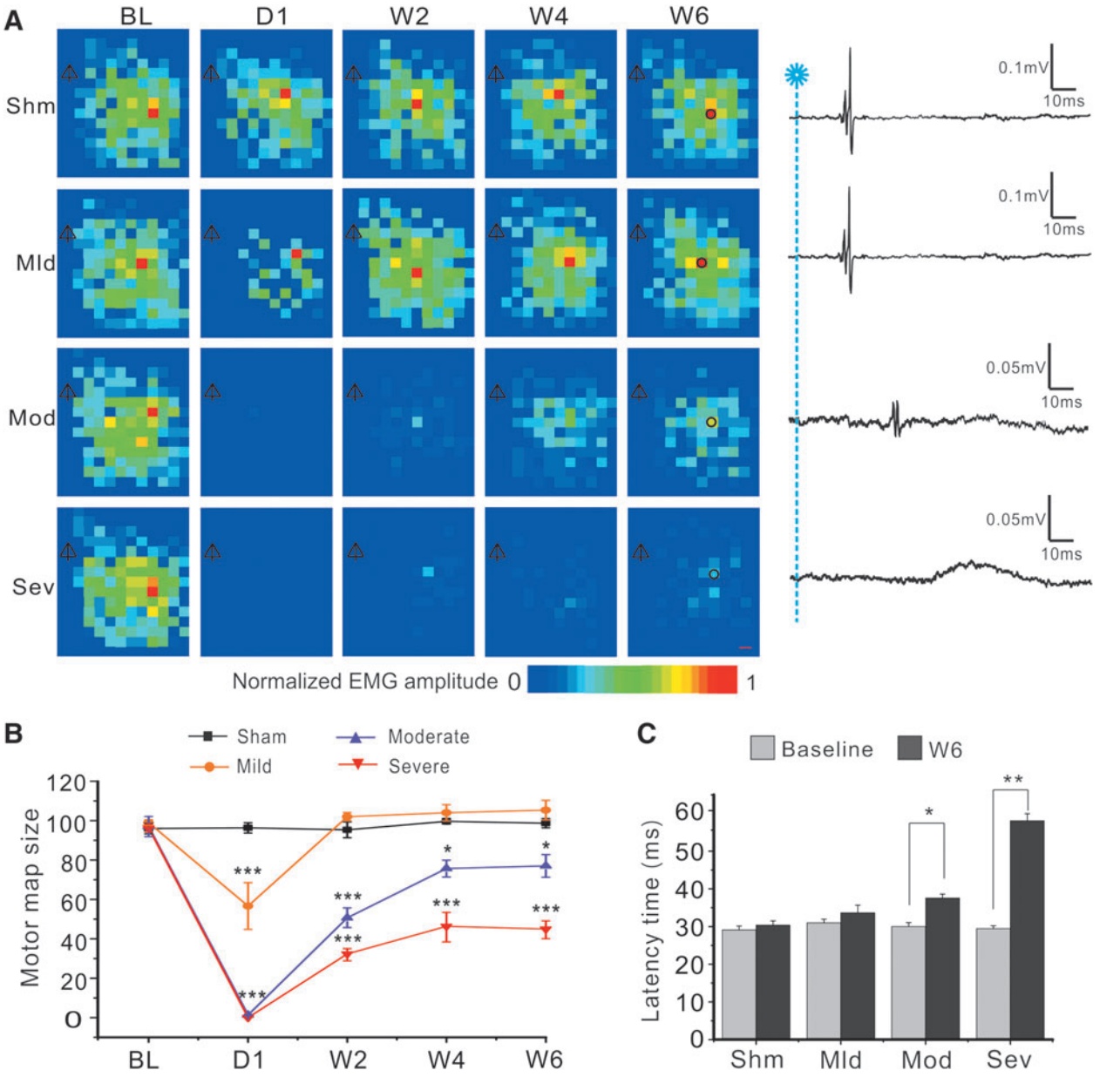

FIG. 2. Longitudinal optogenetic mapping revealed initial loss and subsequent recovery of cortical motor map after different severities of spinal cord contusion. (**A**) Representative motor maps at baseline, 1 day, and 2, 4, and 6 weeks after sham (Shm) and mild (Mld), moderate (Mod), and severe (Sev) SCI, respectively. Distances between neighboring spots were 300 μm. The scale bar at the bottom represents different amplitudes of evoked EMG normalized to maximal response. Shown on the right column are representative EMG traces at 6 weeks after SCI, which correspond to the black circles of the W6 maps of the same row. Note the greatly decreased amplitudes and increased latencies of the responses in the moderate and severe SCI groups 6 weeks after surgery. ⏃, bregma. (**B**) Changes in mean motor map sizes as represented by total numbers of responsive spots in each map. There were different losses of motor map at 1 day after SCI, which were followed by different and gradual recovery of the maps in different groups in 6 weeks. $*p<0.05$; $**p<0.01$; $***p<0.001$, when compared to the sham group. (**C**) At 6 weeks after injury, mean latency periods in the moderate and severe SCI groups were significantly longer than those of the baseline. EMG, electromyogram; SCI, spinal cord injury. Color image is available online at www.liebertpub.com/neu

device, two holes were drilled on the skull, with one above the hindlimb area of the motor cortex for stimulation (bregma –0.8 mm and lateral 1 mm) and the other above the red nucleus (bregma 3.5 mm and lateral 0.5 mm) for recording evoked responses. After a concentric bipolar electrode (FHC, Inc., Bowdoin, ME) was lowered into the motor cortex to a depth of 600–700 μm and a tungsten microelectrode (WPI, Sarasota, FL) was lowered to a depth of 3400 μm, single electrical pulses were applied (200 μs at 0.2–10.0 mA) to the stimulating electrode once every 15 sec. For each mouse, stimulus intensity was started from 0.2 mA and gradually increased to up to 10 mA. Response thresholds were determined when around 50% of the stimuli induced responses. Once the threshold stimulus intensity was determined, increasing stimulating currents at 2, 4, 8, 16, and 32 times the threshold were applied to determine a stimulus-response relationship. Responses were amplified at 100×, digitized, and saved to a computer. For analysis,

responses from 30 repetitions at each intensity were averaged and peak amplitude and latency were measured in Clampfit software.

Statistical analysis

All data are presented as mean ± standard error of the mean. One- or two-way analysis of variance (ANOVA) followed by Tukey's post-hoc analysis or Student's *t*-test were used to evaluate statistical significance. Correlation coefficients were calculated as Pearson correlation coefficients (R) and as multiple linear regression correlation coefficients (R^2). Pearson correlations were performed between motor map size and behavioral scores, and between motor map size and neurons labeled with FG in the red nucleus. All statistical values were calculated using GraphPad Prism software (version 7.0; GraphPad Software, Inc., La Jolla, CA), and $p < 0.05$ was considered statistically significant.

Results

Longitudinal optogenetic mapping of motor cortex revealed loss and partial recovery of motor map after graded contusive spinal cord injury

We used a blue laser to stimulate the left motor cortex of Thy-ChR2 transgenic mice and recorded EMG signals of the right hindlimb, from which motor maps were constructed based on cumulative EMG amplitude at each stimulating spot (Fig. 2A). In the sham group, sizes and distributions of motor maps did not change significantly at different time points in 6 weeks after surgery ($p > 0.05$; Fig. 2A,B), suggesting that optogenetic motor mapping was reliable for chronic longitudinal evaluation of motor pathway function. Three groups of mice ($n = 8$ in each group) received mild, moderate, and severe contusive SCI by varying the impact force of the IH device. EMG amplitude and size of motor maps decreased dramatically at day 1 after SCI, with the mild SCI group having the least decrease and the moderate and severe SCI groups having the most decreases in map size (Fig. 2A,B). Motor maps then gradually and partially recovered in 2, 4, and 6 weeks post-injury. In the moderate and severe SCI groups, EMG events in the mapping area often had longer latencies and smaller amplitudes. They had normal waveforms or abnormal waveforms with longer duration and slower rise and decay times (Fig. 2A,C).

Motor maps of the mild SCI group became similar to baseline in 2 weeks after SCI (Fig. 2A,B; $p > 0.05$ at 2, 4, and 6 weeks after SCI when compared to the sham group), but those of the moderate and severe SCI groups only partially recovered, with the severe SCI group having the lowest EMG amplitude and least responsive spots even at 6 weeks post-SCI (Fig. 2A,B; $p < 0.001$, $p < 0.01$, and $p < 0.01$ at 2, 4, and 6 weeks, respectively, for both the moderate and severe SCI groups when compared to the sham group; two-way ANOVA followed by Tukey's post-hoc analysis). Motor map size of the severe SCI group was significantly smaller than that of the moderate SCI group (Fig. 2B; $n = 8$; $p < 0.05$, $p < 0.01$, and $p < 0.01$ at 2, 4, and 6 weeks, respectively). Results indicate that loss of cortical motor map reflected severity of SCI.

We calculated average latency periods at baseline and 6 weeks after SCI. At baseline, evoked EMG had a mean latency of 29.1 ± 1.0 ms. In mild SCI mice, latency of EMG at 6 weeks post-injury was normal (Fig. 2C; $n = 8$; $p > 0.05$, Student's *t*-test). However, latency periods of the moderate and severe SCI groups at 6 weeks post-injury became significantly longer than that of baseline (37.6 ± 1.2 ms in moderate SCI group and 58.1 ± 1.8 ms in severe SCI group; $p < 0.05$ and $p < 0.01$; Fig. 2C). Results indicate that SCI caused a longer EMG latency period and such change was related to severity of SCI.

We also analyzed average EMG amplitudes at different time points along medial-lateral (Fig. 3A) and anterior-posterior axes (Fig. 3B) and compared them among the four groups. At baseline, evoked EMG had a maximal amplitude of 0.21 ± 0.06 mV. Similar to changes in map size, average amplitudes decreased dramatically at 1 day after injury and recovered partially over time in SCI animals. Average amplitudes of the mild SCI group recovered to almost normal level 2 weeks after injury, but amplitudes of the moderate and severe SCI groups only recovered partially 2, 4, and 6 weeks after injury (Fig. 3C). Changes in EMG amplitudes were similar along anterior-posterior and medial-lateral directions (Fig. 3).

Positive correlations between motor map size and motor function after spinal cord injury

To determine whether optogenetic motor mapping could reflect motor functional deficit and recovery post-SCI, we performed BMS, rota-rod, and grid walk tests simultaneously during longitudinal optogenetic motor mapping. In the BMS test, we found that the three SCI groups showed different degrees of motor impairments after injury, with increasing reduction of BMS scores from mild to moderate and severe SCI groups (Fig. 4A). BMS scores of the mild SCI group returned to almost baseline level 2 weeks post-injury, but the other two SCI groups showed only partial recovery and did not return to baseline level even at 6 weeks post-injury. There were significant differences in BMS scores when the moderate and severe SCI groups were compared to the sham group at different time points after injury (all $p < 0.001$, two-way ANOVA followed by Tukey's post-hoc analysis); there were also significant differences among the mild, moderate, and severe SCI groups at 2, 4, and 6 weeks after SCI (all $p < 0.001$). Motor map size, as indicated by the number of total responsive spots in each map, was strongly correlated with BMS scores at 2, 4, and 6 weeks after injury (Fig. 4A; Pearson correlation coefficients, $R^2 = 0.87$, $R^2 = 0.84$, and $R^2 = 0.90$ for mild, moderate, and severe SCI groups, respectively; $n = 8$ for each group; all $p < 0.001$). Results indicate that BMS is sensitive in reflecting severity of contusive SCI, and that size of the motor map is highly correlated with loss and spontaneous recovery of BMS scores.

The rota-rod test showed significant deficits in moderate and severe SCI groups after injury. Times spent on the rotating rod of the moderate and severe SCI groups at 2, 4, and 6 weeks post-injury were significantly shorter than those of the sham and mild SCI groups (all $p < 0.001$). There were also significant differences in retention times between the moderate and severe SCI groups at 2, 4, and 6 weeks post-injury ($p < 0.01$, $p < 0.05$, and $p < 0.05$, respectively). However, no significant differences were found in retention times at each testing time point between the mild SCI and sham groups ($p > 0.05$). There were positive correlations between motor map size and retention time in rota-rod test at 2, 4, and 6 weeks after injury ($R^2 = 0.84$, $R^2 = 0.72$, and $R^2 = 0.79$, respectively; all $p < 0.001$; Fig. 4B). Results suggest that the rota-rod test is also sensitive to severity of contusive SCI, and that size of motor mapping is highly correlated with loss and spontaneous recovery of retention time of rota-rod test.

In the grid walk test, there were significant differences in numbers of footfalls of the severe SCI group at 2, 4, and 6 weeks post-injury when compared to all other groups ($p < 0.001$ at each time point). There were also significant differences in the number of footfalls of the moderate SCI group at 2 weeks post-injury when

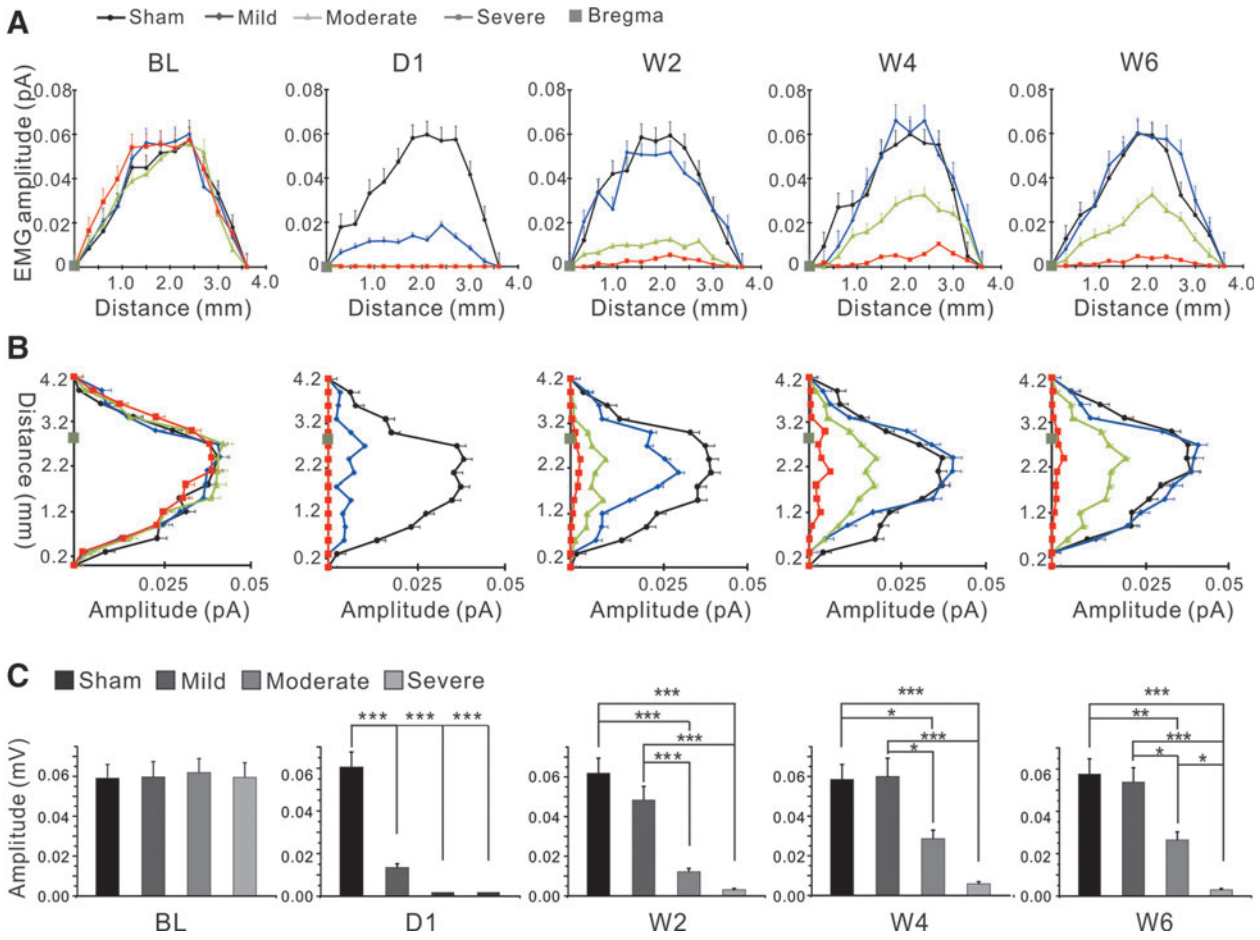

FIG. 3. Reduced EMG amplitudes of motor maps after SCI. (**A**) Comparisons among all groups of average peak amplitudes of responsive spots along medial-lateral axes of the mapping areas. (**B**) Comparisons among all groups of average peak amplitudes of responsive spots along anterior-posterior axes of the mapping areas. In both directions, there were great decreases in amplitudes on day 1 post-SCI and gradual recovery in 2, 4, and 6 weeks post-SCI in all injured groups, with the mild SCI > moderate SCI > severe SCI group in recovery. (**C**) Mean amplitudes of responsive spots of individual maps at baseline, 1 day, and 2, 4, and 6 weeks after SCI. $*p<0.05$; $**p<0.01$; $***p<0.001$, one-way ANOVA. ANOVA, analysis of variance; EMG, electromyogram; SCI, spinal cord injury. Color image is available online at www.liebertpub.com/neu

compared to the sham and mild SCI groups (both $p<0.05$). However, there were no significant differences in numbers of footfalls of the moderate SCI group at 4 and 6 weeks post-SCI and those of the mild SCI group at all time points when compared to the sham group (Fig. 4C). There were negative correlations between motor map size and footfalls tested by grid walk at 2, 4, and 6 weeks after injury ($R^2=-0.62$, $R^2=-0.45$, and $R^2=-0.67$, respectively; all $p<0.001$; Fig. 4C). Results indicated that the grid walk test was less sensitive in reflecting motor impairment after mild and moderate contusive SCI, and that size of the motor map is inversely correlated with the percentage of footfalls in the grid walk test.

A negative correlation between lesion area of the spinal cord and motor map size after spinal cord injury

To determine whether optogenetic motor mapping could reflect structural damage of the spinal cord, we examined the lesion area of injured spinal cord at 6 weeks after SCI and analyzed its correlation with motor map size at that time point. Staining of spinal cords using cresyl violet and eosin showed an increment of lesion area at the epicenter of the injured spinal cord that corresponded to severity of SCI (Fig. 5A). Percentages of lesion areas at the epicenter of the mild, moderate, and severe SCI groups were $15.5\pm2.3\%$, $63.4\pm5.5\%$, and $91.5\pm1.9\%$, respectively (Fig. 5B; all $p<0.001$ when they were compared with one another; $n=8$ in each group; one-way ANOVA followed by Tukey's post-hoc analysis). Correlation analysis showed that the lesion area of injured spinal cord at 6 weeks post-injury was negatively correlated with the size of the motor map at that time point ($R^2=-0.85$; $p<0.001$; Fig. 5C). Results suggest that optogenetic motor mapping reflects the severity of chronic structural damage of the spinal cord after SCI.

Different impairments of corticospinal tract and rubrospinal tract in 6 weeks after spinal cord injury

To examine the damage of CST and RST caused by graded contusive SCI and their potential correlation with motor map size, we used FG to retrogradely label neurons in the motor cortex and midbrain red nucleus in 6 weeks after SCI. In the uninjured motor cortex, CST neurons that were labeled by FG were confined to layer

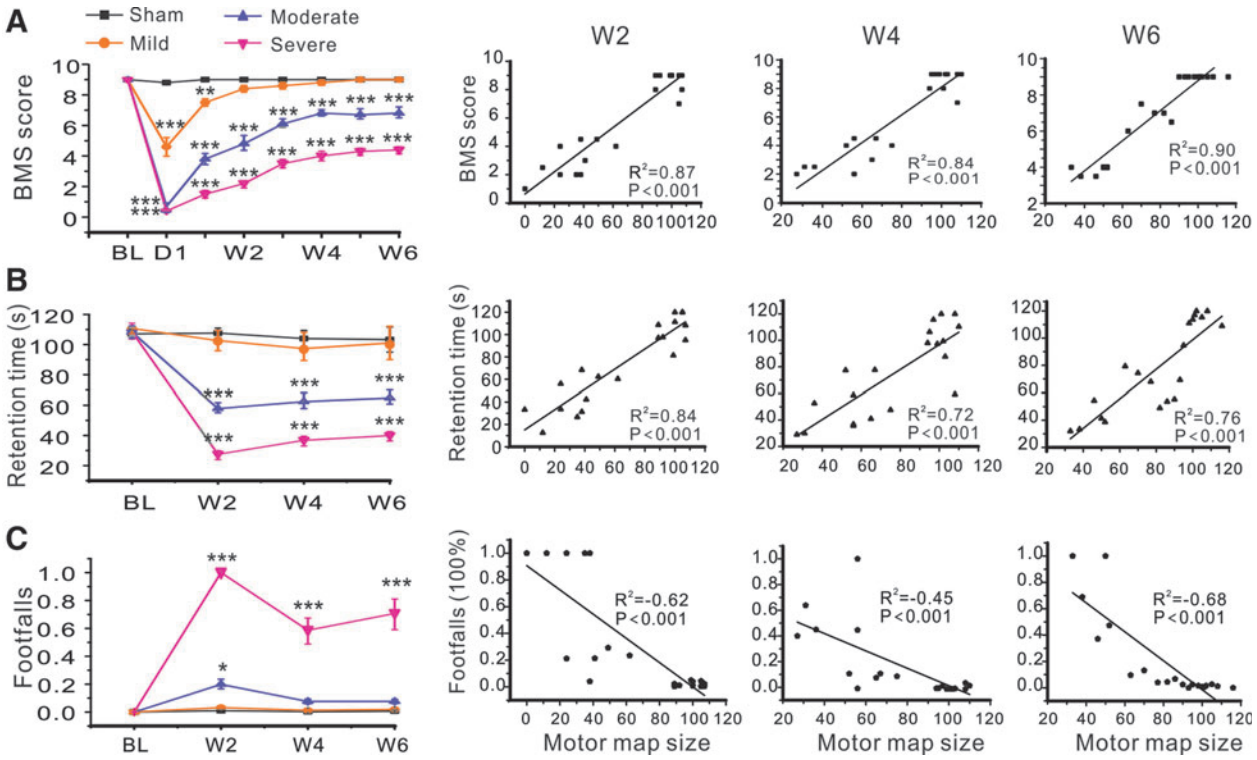

FIG. 4. Correlations between motor map size and motor behavioral performance at different time points following SCI. (**A**) Results of BMS test and their correlations with motor map size at 2, 4, and 6 weeks after SCI. (**B**) Results of rota-rod test and their correlations with motor map size at 2, 4, and 6 weeks after SCI. (**C**) Results of grid walk test and their correlations with motor map size at 2, 4, and 6 weeks after SCI. *$p<0.05$; **$p<0.01$; ***$p<0.001$, when compared to the sham group. BMS, Basso Mouse Scale; SCI, spinal cord injury. Color image is available online at www.liebertpub.com/neu

V (Fig. 6A). SCI caused a dramatic loss of FG labeling in the motor cortex, with only a few neurons labeled after mild SCI and no neurons labeled after moderate or severe SCI (all $p<0.001$; Fig. 6A,B). Correlation analysis showed that the number of FG-labeled CST neurons at 6 weeks post-injury was not correlated with motor map size ($p>0.05$, data not shown). In red nucleus of the sham group, neurons labeled by FG were mostly located in the caudal part of the magnocellular red nucleus (Fig. 6A). SCI caused significant reductions of FG-labeled neurons in red nucleus in all injured groups, with the mild SCI group having the most FG-labeled neurons and the severe SCI group having the fewest (Fig. 6A,C). Specifically, there were significant differences in numbers of FG-labeled neurons in red nucleus between the moderate or severe SCI group and the sham or mild SCI group (all $p<0.001$) and between the moderate and severe SCI groups ($p<0.01$; Fig. 6C). However, there was no significant difference in FG-labeled neurons in red nucleus between the sham and mild SCI groups ($p>0.05$; Fig. 6C). Correlation analysis showed that the number of FG-labeled neurons in red nucleus at 6 weeks post-injury were strongly and positively correlated with motor map size ($R^2=0.82$; $p<0.001$; Fig. 6D), suggesting that optogenetic motor mapping reflects preservation of RST, but not CST, innervation during chronic stage after contusive SCI.

Motor cortical stimulation activated more neurons in red nucleus after spinal cord injury

Expression of c-Fos protein is associated with neural and behavioral activity in response to acute stimulation and is commonly used as a marker of neuronal activation.[37] To evaluate potential circuit reorganization from motor cortex to subcortical targets after SCI, we prepared a moderate SCI group and a sham injury group of ChR2 mice and used a miniature LED for optogenetic stimulation of the motor cortex to examine c-Fos expression in motor cortex and subcortical nuclei, including the red nucleus. In the motor cortex, optogenetic stimulation resulted in significant increases in density of c-Fos–positive cortical cells in both the sham and SCI groups (Fig. 7A,B; both $p<0.01$ when compared with contralateral sides of the sham and SCI groups, respectively). However, densities of c-Fos–expressing neurons between the sham and SCI groups after stimulation were similar (Fig. 7A,B; $n=5$ in each group; $p>0.05$, one-way ANOVA followed by Tukey's post-hoc test).

In the red nucleus, c-Fos–expressing neurons were located in rostral and caudal parts of the nucleus. In contrast to results of the motor cortex, optogenetic stimulation resulted in a higher density of c-Fos–expressing neurons in the SCI group than that in the sham group (Fig. 7C,D; $p<0.05$.). Results indicate enhanced functional corticorubral connectivity in the red nucleus after moderate contusive SCI.

Spinal cord injury caused denser corticorubral axons and synapses in red nucleus

To determine structural plasticity of corticorubral pathway after SCI, we simultaneously injected FG into the spinal cord for retrograde labeling of rubrospinal neurons and BDA into the motor cortex for anterograde tracing of corticorubral axons in the red nucleus after injury. In comparison to the sham group, a higher density of axons

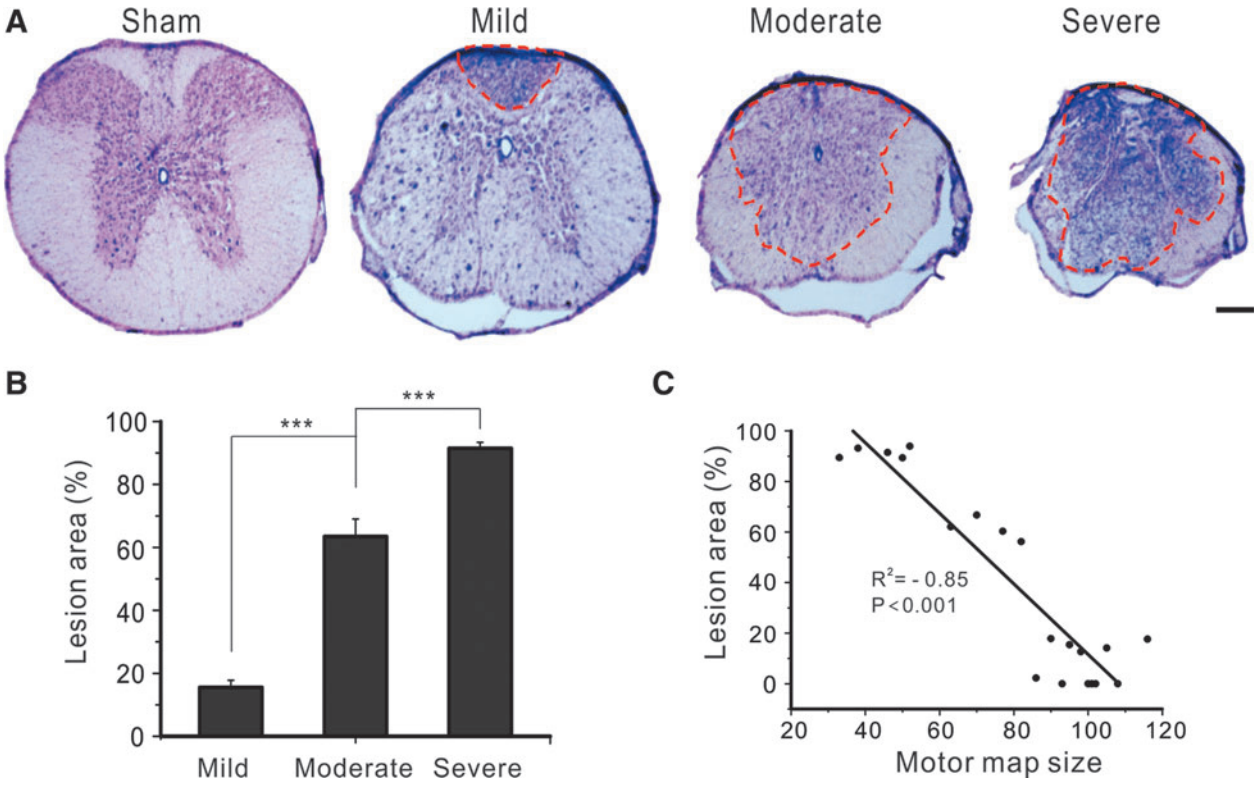

FIG. 5. Motor mapping reflected structural damage of the spinal cord after contusive SCI. (**A**) Cross-sectional images of spinal cords at levels of lesion epicenter after different severities of spinal cord contusion. Dotted red lines outline the lesion areas. (**B**) Mean lesion areas at levels of epicenter after mild, moderate, and severe SCI. ***$p < 0.001$. Scale bar, 50 μm. (**C**) There is a negative correlation between motor map size at 6 weeks after SCI and the lesion areas of the injured spinal cord. SCI, spinal cord injury. Color image is available online at www.liebertpub.com/neu

was labeled by BDA in the red nucleus in the SCI group (Fig. 8A). Relative fluorescence intensity of BDA-labeled axons in the red nucleus was significantly higher in the SCI group than in the sham group (Fig. 8B; 182.7 ± 23.6 arbitrary units [AU] in the sham group vs. 409.4 ± 41.3 AU in the SCI group; $n = 5$; $p < 0.001$, Student's t-test).

To further determine whether corticorubral axons made more synapses with rubrospinal neurons in the red nucleus after SCI, we combined anterograde tracing of corticorubral axons and retrograde tracing of rubrospinal neurons with immunostaining of synapse marker synaptophysin to analyze the number of putative corticorubral synapses on the somata of red nucleus neurons. We found that the number of triple-labeled putative synapses per FG-positive cell in the moderate SCI group was significantly higher than that of the sham group (4.25 ± 0.69 in sham group vs. 11.78 ± 1.38 in SCI group; $n = 5$; $p < 0.01$; Fig. 9A,B).

Stronger corticorubral synaptic connection in spinal cord injury mice in vivo

To determine whether increased corticorubral fibers and synapses would result in a stronger synaptic connection between these two structures, we made *in vivo* extracellular recordings at 6 weeks after moderate SCI by stimulating motor cortex and recording in the red nucleus. Focal electrical stimulation of the hindlimb region of the motor cortex evoked, in the red nucleus, post-synaptic potentials that were dependent on electrode depth and direction as well as stimulus intensity (Fig. 10A,B). The threshold for inducing synaptic response in the SCI group was significantly lower than that in the sham group (Fig. 10B; 0.68 ± 0.04 and 0.29 ± 0.01 mA for the sham and SCI groups, respectively; $n = 5$ for both groups; $p < 0.001$, Student's t-test), and the response amplitude of the SCI group was significantly larger than that of the sham group (Fig. 10C; 0.6 ± 0.03 and 0.76 ± 0.02 mV for the sham and SCI groups, respectively; $p < 0.01$). However, there was no significant difference in latency period between the two groups (Fig. 10D; 4.5 ± 0.27 and 4.26 ± 0.15 ms for the sham and SCI groups, respectively; $p > 0.05$). Results indicate that corticorubral projection makes stronger synaptic coupling after SCI.

Discussion

In this study, we showed that graded contusive SCI caused different severities of structural damage of the spinal cord, loss of corticorubrospinal projection, and impairment of motor function, as revealed by tissue histology, tract tracing, and BMS, rota-rod, and grid walk tests. All these changes were highly correlated with map size of *in vivo* longitudinal optogenetic motor mapping, suggesting that optogenetic motor mapping is sensitive and useful for functional evaluation of impairment and plasticity of the spinal cord after SCI. We also found that motor cortex after chronic SCI made stronger functional connections with the red nucleus, which was achieved by sending denser conticorubral axons and forming more synapses onto rubrospinal neurons in the red nucleus. Enhanced corticorubrospinal projection likely contributes to spontaneous motor functional recovery after contusive SCI.

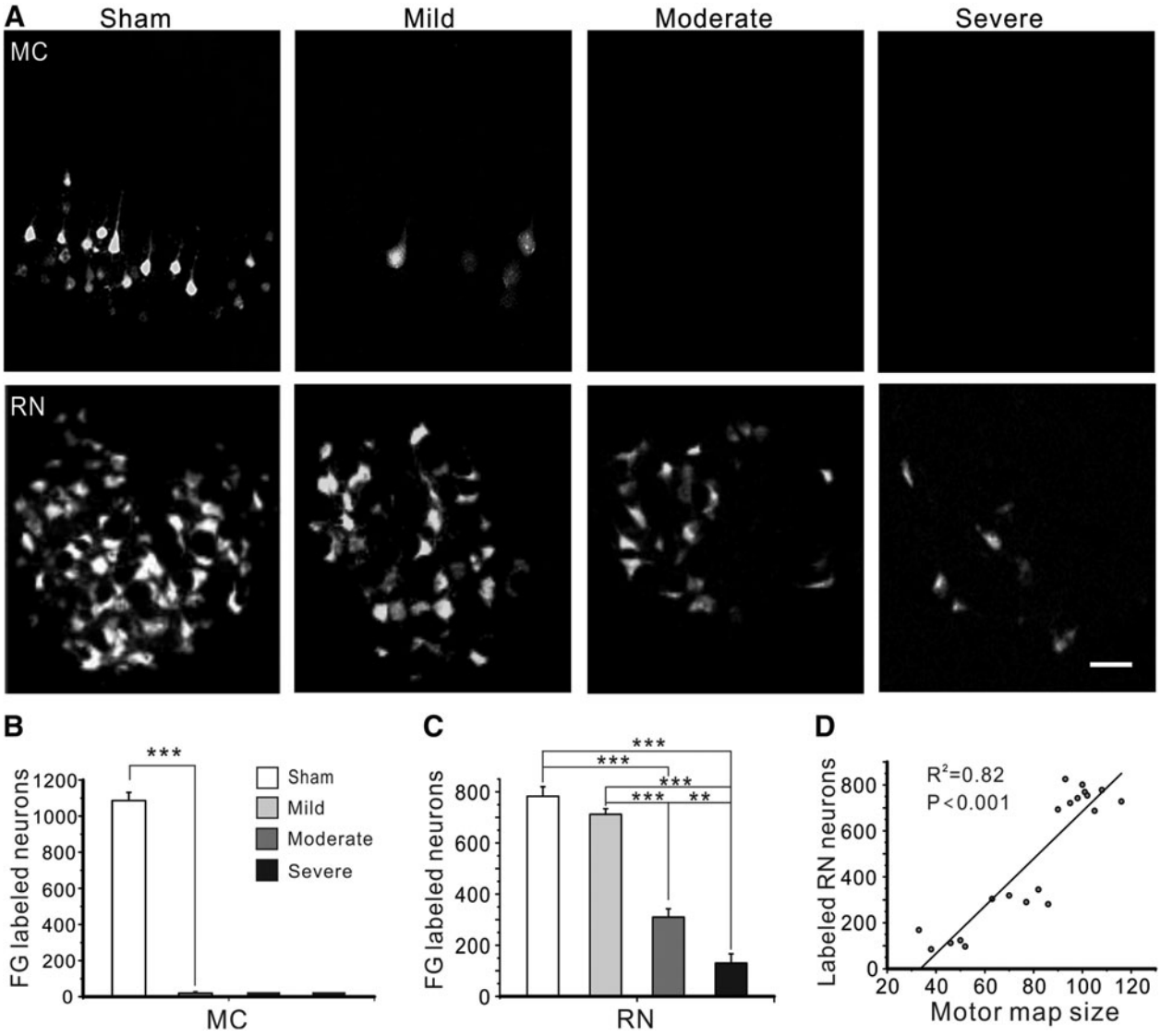

FIG. 6. Graded SCI had different impacts on cortico- and rubrospinal projections. (**A**) Representative fluorescence images showing reduced number of neurons that were retrogradely labeled by FG in motor cortex (MC; top row) and red nucleus (RN; bottom row) at 6 weeks after mild, moderate, and severe SCI. Scale bar, 100 μm. (**B** and **C**) Mean numbers of FG-labeled neurons in the motor cortex (B) and magnocellular red nucleus (C) at 6 weeks after SCI in all groups. In the motor cortex (MC), even mild SCI caused almost complete loss of retrogradely labeled CST neurons. In contrast, the numbers of FG-labeled neurons in the RN gradually decreased with increasing severity of SCI. (**D**) There exists a strong negative correlation between motor map size at 6 weeks after surgery and the number of neurons labeled by FG in red nucleus. $^{**}p < 0.01$; $^{***}p < 0.001$. CST, corticospinal tract; FG, Fluoro-Gold; SCI, spinal cord injury.

In Thy1-ChR2-YFP transgenic mice, cortical layer V ChR2-expressing neurons and their connected subcortical projections (including CST and corticorubrospinal tract) can be activated with blue light to evoke motor response and motor maps can be constructed based on the physical movement of a limb or evoked EMG of a target muscle.[17,19,20] We adapted a laser scanning photostimulation system that was originally designed for glutamate uncaging for *in vivo* motor mapping.[31,32] The system used a pair of galvanometer mirrors to quickly scan a rectangular area of 1.2×1.5 mm with 300-μm spacing under a $5\times$ objective (Fig. 1). Because this scanning area only covered a portion of fore- or hindlimb motor cortex, we made two medial-lateral rows of three mapping areas each to cover a whole limb area and merged them together to form a complete motor map. Motor maps generated this way are comparable to optogenetic maps made by other labs and motor maps generated with a cortical electrical stimulation technique.[19,20,38] Results of the optogenetic motor map in sham mice had a similar size and pattern at different time points at 6 weeks, supporting a good reliability of this technique in detecting a motor map over time.

We found that longitudinal optogenetic mapping allows measuring injury severity and dynamic recovery of descending motor pathway after SCI. A previous study in rats established a relationship between SCI severity and preservation of axons and motor function so that severer spinal cord contusion causes greater decrease in axon preservation and poorer motor function.[39] In our

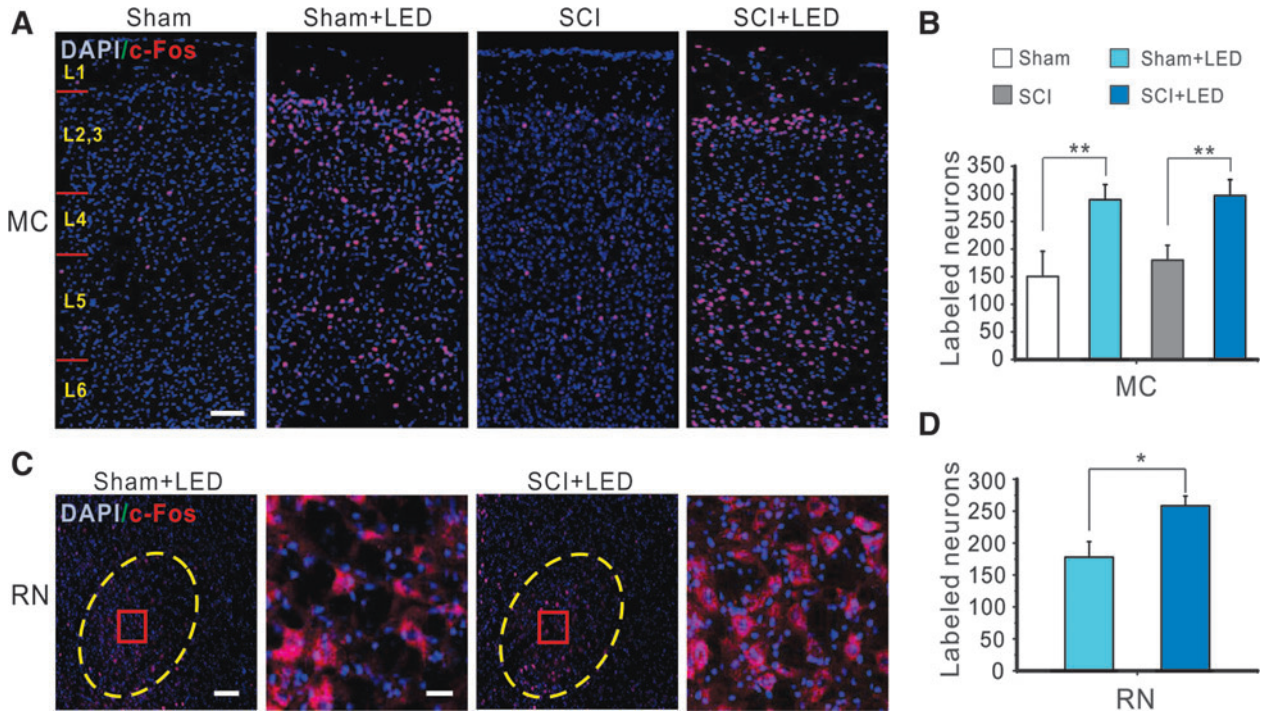

FIG. 7. Optogenetic stimulation of motor cortex (MC) activated more c-Fos–expressing neurons in red nucleus (RN) in SCI mice than in sham-injured mice. (**A** and **B**) At 6 weeks after sham injury or moderated SCI, optogenetic stimulation of the motor cortex using a blue LED for 30 min resulted in significant increases in the numbers of c-Fos–positive neurons per section in the motor cortex in both groups. However, the numbers of c-Fos–positive neurons per section were similar in the sham and SCI groups after optogenetic stimulation. (**C** and **D**) In contrast, cortical optogenetic stimulation activated a greater number of c-Fos–positive neurons per section in red nucleus of the SCI group than that of the sham group. Scale bars, 50 μm for low-power images of (A) and (C); 20 um for enlarged image of (C); $n=5$ mice in each group. *$p<0.05$; **$p<0.01$, Student's t-test. DAPI, 4',6-diamidino-2-phenylindole; LED, light-emitting diode; SCI, spinal cord injury. Color image is available online at www.liebertpub.com/neu

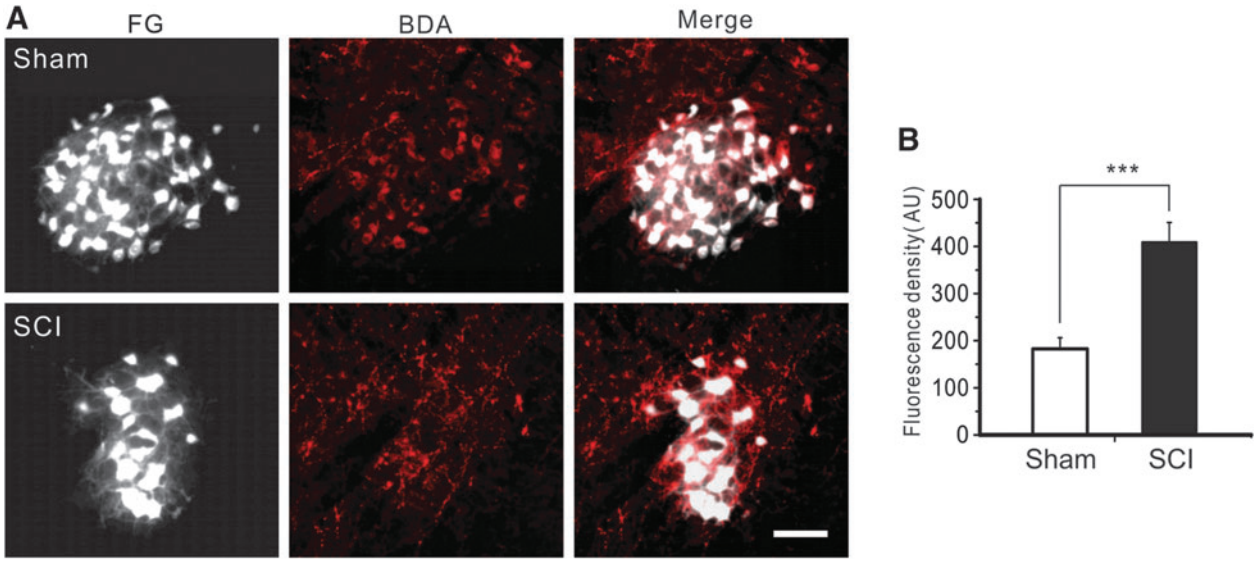

FIG. 8. Enhanced projection of corticorubral axons after SCI. (**A**) In sham (top row) and SCI (bottom row) mice, rubrospinal neurons that were retrogradely labeled with FG in the red nucleus were greatly reduced after SCI (left column), but corticorubral axons that were anterogradely labeled with injection of BDA in the motor cortex became denser after SCI (middle and right columns). (**B**) Fluorescence density was significantly higher in the SCI group than the sham group; $n=5$ in each group; ***$p<0.001$; scale bar, 50 μm. AU, arbitrary units; BDA, biotin dextran amine; FG, Fluoro-Gold; SCI, spinal cord injury. Color image is available online at www.liebertpub.com/neu

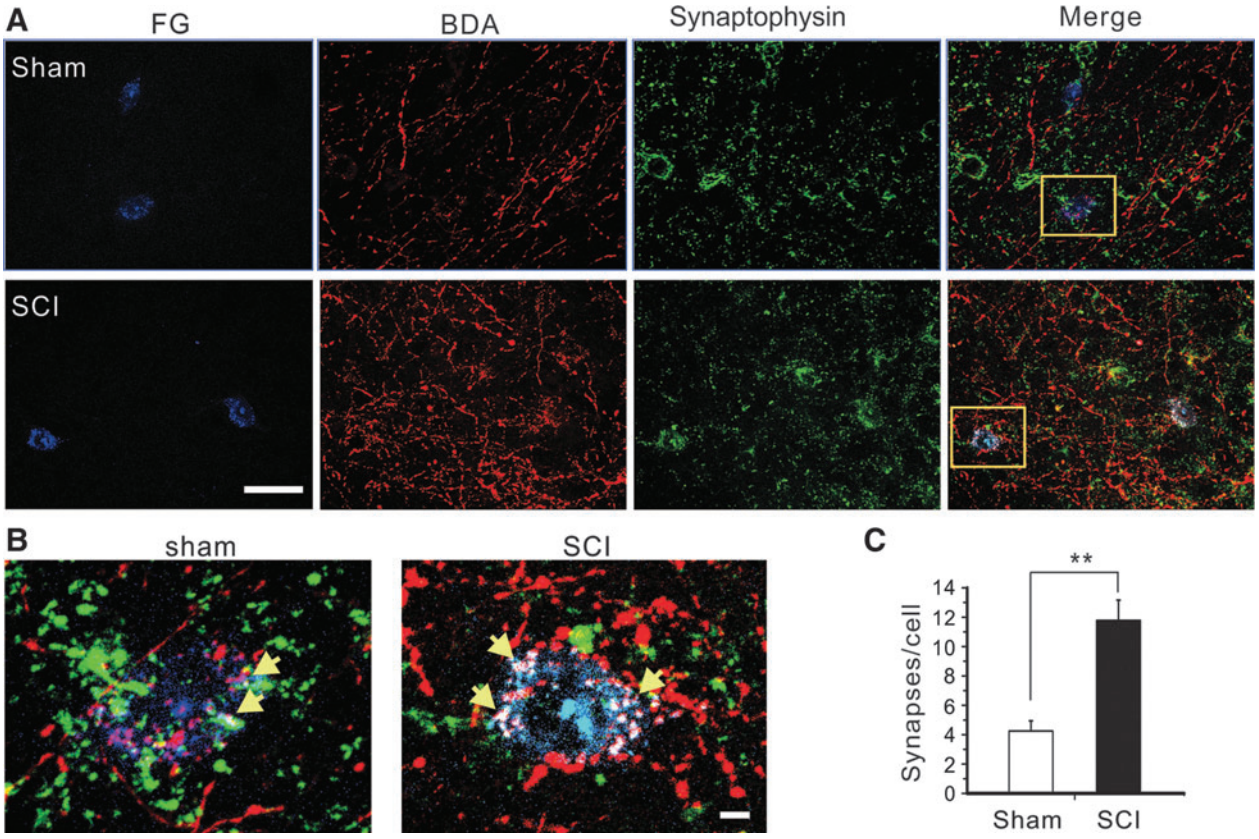

FIG. 9. Increased density of corticorubral synapses in red nucleus after moderate SCI. (**A**) Representative images showing co-labeling of rubrospinal neurons (FG), corticorubral axons (BDA), and synaptophysin immunostaining in red nucleus in the sham group (top) and moderate SCI group (bottom). (**B**) The number of corticorubral synapses on rubrospinal neurons of the red nucleus at 6 weeks after SCI was significantly higher than that of the sham group ($n=5$; $p<0.01$, Student's t-test). Scale bars: (A), 50 μm; (B), 5 μm. BDA, biotin dextran amine; FG, Fluoro-Gold; SCI, spinal cord injury. Color image is available online at www.liebertpub.com/neu

study, the immediate loss of cortical motor map induced by graded contusive SCI was highly correlated with injury severity. The changes in motor map size after contusive SCI were highly correlated with the changes in motor performance assessed by the BMS and rota-rod tests. A strong negative correlation was also found between lesion area of injured spinal cord and motor map size at 6 weeks after SCI. Could neuronal death in the related brain structures contribute to the loss of motor map? Whereas some studies did not find early death of cortico- and rubrospinal neurons after SCI, others demonstrated early death of $\sim$5% or fewer motor cortical neurons and chronic degeneration (in 6–8 weeks) of as many as 51% rubrospinal neurons.[40–43] Given the small percentage of cell death in the motor cortex and late onset of degeneration in the red nucleus, their contribution to motor map loss is likely small. Thus, motor map loss can be mainly attributed to direct damage of SCI to spinal cord motor tracts. These results support that optogenetic motor mapping reflects severity of SCI and motor recovery; thus, it can be used as a functional measurement for both structural and functional impairment and plasticity during the acute and chronic phases after contusive SCI.

The observed spontaneous functional recovery, particularly the recovery of motor map, suggests likely plasticity and reorganization of the motor pathway from the motor cortex to injured spinal cord, which is known to be an important mechanism after SCI.[6–8,10] Both the CST and corticorubrospinal tract have a prominent role in controlling voluntary skilled movements of limbs.[22,23,44] In adult mice, SCI that involves a lesion of dorsal column could damage up to 96% of CST fibers.[17] Although preservation of dorsolateral CST was found to contribute to spontaneous motor recovery after dorsal column SCI,[17] our retrograde tracing results showed no FG-labeled neurons in the motor cortex after moderate and severe contusive SCI, suggesting that the CST was completely damaged in this model and was unlikely to play a significant role in the observed spontaneous functional recovery. Consistently, motor function after spinal cord contusion in rats was found to be highly correlated with integrity of nonpyramidal tracts, particularly the rubrospinal, vestibulospinal, and raphespinal tracts.[39] Carmel and colleagues found that motor functional recovery cannot be fully mediated by spontaneous sprouting of the ipsilateral CST occurring after an incomplete injury, and that corticorubral projections to the magnocellular red nucleus occurring after motor cortex stimulation could provide much help to restore motor function to the affected limb after chronic CST injury.[45] Therefore, spontaneous motor recovery in moderate and severe SCI mice may be explained at least partially by plasticity of spared corticorubrospinal pathway.

The corticorubrospinal tract is a corticofugal pathway that originates from the motor cortex and projects to the red nucleus and then to the spinal cord.[45,46] The red nucleus consists of the parvocellular red nucleus and magnocellular red nucleus. In rats, corticorubral projection terminates within the parvocellular part of the red nucleus.[46,47] However, corticorubral projection in the parvocellular red nucleus does not project to the spinal cord, whereas axons of the

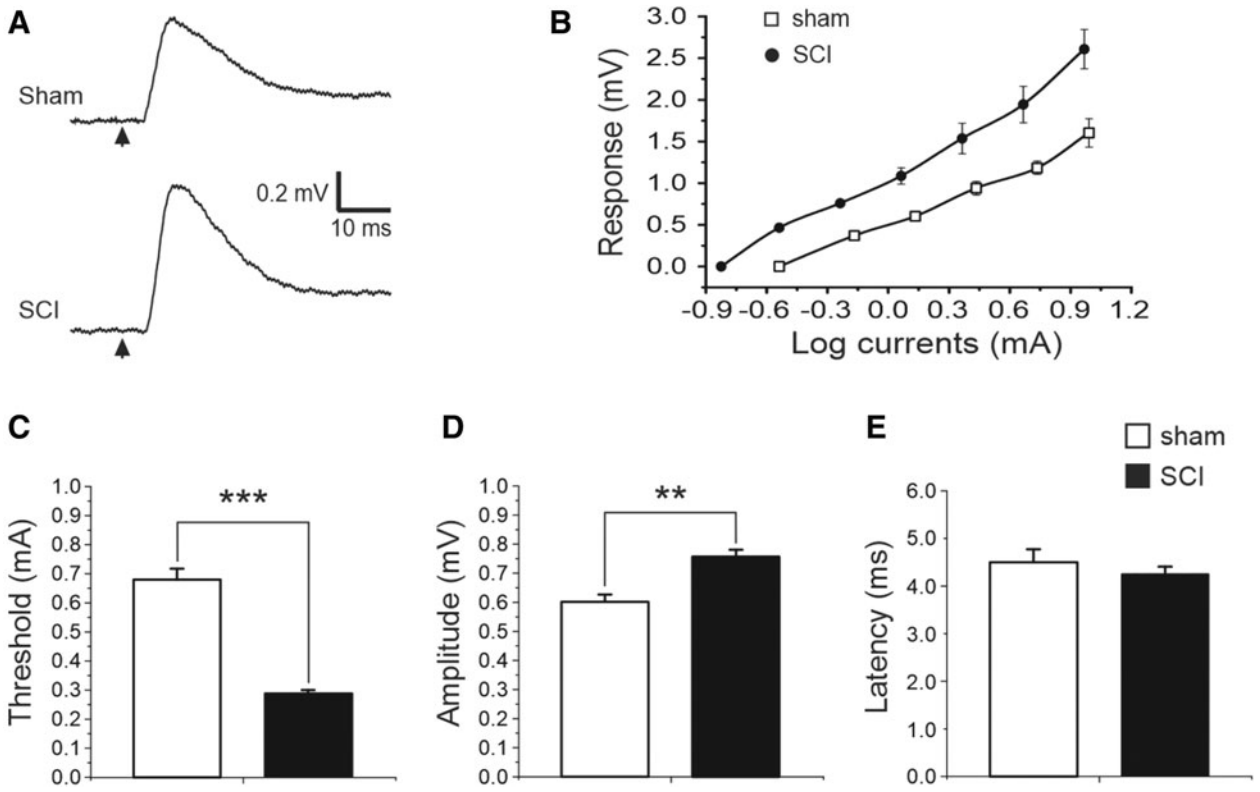

FIG. 10. Stronger corticorubral synaptic connection in red nucleus after moderate SCI. (**A**) Electrical stimulation of motor cortex (arrows) at 2×threshold level induced post-synaptic responses in red nucleus in both sham (top trace) and SCI (bottom trace) mice *in vivo*, but response amplitude of the SCI mouse was higher than that of the sham-injured mouse. (**B**) Relationship between stimulating currents and evoked corticorubral responses in sham and SCI mice. Responses at different stimulation intensities of SCI mice were much larger than those of sham mice. (**C–E**) The threshold for inducing corticorubral response in the SCI group was significantly lower (B, $p < 0.001$, Student's *t*-test) and the amplitude of the synaptic response was significant higher (C; $p < 0.01$) than the sham group, but there was no significant difference in the latency period between the two groups (D, $p > 0.05$); $n = 5$ mice for both groups. SCI, spinal cord injury.

magnocellular red nucleus project down to the spinal cord and are involve in the motor circuit.[46] A relative paucity of cortical projections to the caudal magnocellular red nucleus was also shown in normal North American opossums.[47,48] In our study, increased corticorubral axons in the red nucleus in SCI mice suggest plasticity of this pathway. More important, most BDA-positive corticorubral axons were located at the caudal part of the magnocellular red nucleus, where they co-localized with the rubrospinal neurons retrogradely labeled by FG (Figs. 6 and 7). Because synaptophysin is specifically expressed in vesicles of pre-synaptic terminals and its immunostaining detects both existing and new synapses,[49–51] the increased number of synaptophysin-positive puncta on BDA-labled axons suggests a possible increase in the number of putative corticorubral synapses in the red nucleus. Given that formation of new synapses underlies behavioral improvement,[52] an increase in corticorubral synapses on FG-labeled neurons in the red nucleus would support functional recovery of the reorganized corticorubrospinal tracts. Our electrophysiological recording data further demonstrated that corticorubral connection after SCI has increased excitability and efficacy, as indicated by the lower threshold and higher amplitude of response, respectively (Fig. 10).

Because the RST was shown to originate from the caudal magnocellular red nucleus,[46] the increased corticorubral projection to caudal magnocellular red nucleus may enhance the circuit from the motor cortex to red nucleus and contribute to functional recovery. In support of this, enhancing corticorubral sprouting by blocking myelin-associated neurite growth inhibitors was shown to restore skilled forelimb use in a unilateral pyramidotomy model of SCI in adult rats.[25] In a unilateral ischemic stroke model, treatment with human adult bone-marrow–derived somatic cells promotes recovery of skilled forelimb motor function, which is positively correlated with increased axonal outgrowth of the intact, uninjured corticorubral tract.[53] Conversely, partial recovery of voluntary control of arm and foot in monkeys subjected to unilateral CST lesion disappears when the red nucleus innervating the affected side is lesioned.[54,55] These findings support that sprouting of the corticorubral tract may be an anatomical substrate for motor functional recovery after cortical or spinal cord lesion. Consistently, plasticity of rubrospinal projection after SCI has also been demonstrated in a recent study showing sprouting of rubrofugal and -spinal projections and formation of a new circuit between the red nucleus and the nucleus raphe magnus, which are believed to contribute to functional recovery after bilateral CST injury.[5] Whereas sprouting or *de novo* formation of other subcortical motor pathways, such as those from the brainstem nuclei, likely makes specific contributions,[3–5] an enhancement of corticorubral and rubrospinal projections together makes a stronger functional motor pathway, which may be a mechanism for spontaneous recovery of motor map and motor function after SCI in adult mice.

In conclusion, we demonstrated that transcranial optogenetic motor mapping is an efficient and sensitive technique for evaluating structural and functional impairments and plasticity after different severities of contusive SCI. Although contusive SCI in mice causes severe damage of the dorsal CST, it enhances corticorubral projection and synaptic efficacy by increasing corticorubral fibers and synapses that terminate in the caudal magnocellular red nucleus. Such plasticity and reorganization of the corticorubral pathway may contribute to spontaneous recoveries of motor circuits and function after SCI.

Acknowledgments

This work was supported, in part, by NIH DA039530, CURE Epilepsy Foundation, and the Indiana Spinal Cord and Brain Injury Research Fund from the Indiana State Department of Health (A70-1-079438, A70-3-079971, and A70-4-079956) to XJ. This work was also supported by National Natural Science Fund of China (81471273). The authors thank Patti Raley for editorial assistance.

Author Disclosure Statement

The authors declare that the research was conducted in the absence of any commercial or financial relationships that could be construed as a potential conflict of interest.

References

1. Darian-Smith, C., Lilak, A., Garner, J., and Irvine, K.A. (2014). Corticospinal sprouting differs according to spinal injury location and cortical origin in macaque monkeys. J. Neurosci. 34, 12267–12279.
2. Reed, J.L., Liao, C.C., Qi, H.X., and Kaas, J.H. (2016). Plasticity and recovery after dorsal column spinal cord injury in nonhuman primates. J. Exp. Neurosci. 10, 11–21.
3. Fink, K.L., and Cafferty, W.B. (2016). Reorganization of intact descending motor circuits to replace lost connections after injury. Neurotherapeutics 13, 370–381.
4. Garcia-Alias, G., Truong, K., Shah, P.K., Roy, R.R., and Edgerton, V.R. (2015). Plasticity of subcortical pathways promote recovery of skilled hand function in rats after corticospinal and rubrospinal tract injuries. Exp. Neurol. 266, 112–119.
5. Siegel, C.S., Fink, K.L., Strittmatter, S.M., and Cafferty, W.B. (2015). Plasticity of intact rubral projections mediates spontaneous recovery of function after corticospinal tract injury. J. Neurosci. 35, 1443–1457.
6. Fouad, K., Pedersen, V., Schwab, M.E., and Brosamle, C. (2001). Cervical sprouting of corticospinal fibers after thoracic spinal cord injury accompanies shifts in evoked motor responses. Curr. Biol. 11, 1766–1770.
7. Ghosh, A., Sydekum, E., Haiss, F., Peduzzi, S., Zorner, B., Schneider, R., Baltes, C., Rudin, M., Weber, B., and Schwab, M.E. (2009). Functional and anatomical reorganization of the sensory-motor cortex after incomplete spinal cord injury in adult rats. J. Neurosci. 29, 12210–12219.
8. Gulino, R., Dimartino, M., Casabona, A., Lombardo, S.A., and Perciavalle, V. (2007). Synaptic plasticity modulates the spontaneous recovery of locomotion after spinal cord hemisection. Neurosci. Res. 57, 148–156.
9. Jayaprakash, N., Wang, Z., Hoeynck, B., Krueger, N., Kramer, A., Balle, E., Wheeler, D.S., Wheeler, R.A., and Blackmore, M.G. (2016). Optogenetic interrogation of functional synapse formation by corticospinal tract axons in the injured spinal cord. J. Neurosci. 36, 5877–5890.
10. Rosenzweig, E.S., Courtine, G., Jindrich, D.L., Brock, J.H., Ferguson, A.R., Strand, S.C., Nout, Y.S., Roy, R.R., Miller, D.M., Beattie, M.S., Havton, L.A., Bresnahan, J.C., Edgerton, V.R., and Tuszynski, M.H. (2010). Extensive spontaneous plasticity of corticospinal projections after primate spinal cord injury. Nat. Neurosci. 13, 1505–1510.
11. Raineteau, O., and Schwab, M.E. (2001). Plasticity of motor systems after incomplete spinal cord injury. Nat. Rev. Neurosci. 2, 263–273.
12. Antal, M. (1984). Termination areas of corticobulbar and corticospinal fibres in the rat. J. Hirnforsch. 25, 647–659.
13. Agrawal, G., Iyer, S., and All, A.H. (2009). A comparative study of recording procedures for motor evoked potential signals. Conf. Proc. IEEE Eng. Med. Biol. Soc. 2009, 2086–2089.
14. McKay, W.B., Stokic, D.S., and Dimitrijevic, M.R. (1997). Assessment of corticospinal function in spinal cord injury using transcranial motor cortex stimulation: a review. J. Neurotrauma 14, 539–548.
15. Zhang, Y.P., and Oertner, T.G. (2007). Optical induction of synaptic plasticity using a light-sensitive channel. Nat. Methods 4, 139–141.
16. Wang, H., Peca, J., Matsuzaki, M., Matsuzaki, K., Noguchi, J., Qiu, L., Wang, D., Zhang, F., Boyden, E., Deisseroth, K., Kasai, H., Hall, W.C., Feng, G., and Augustine, G.J. (2007). High-speed mapping of synaptic connectivity using photostimulation in Channelrhodopsin-2 transgenic mice. Proc. Natl. Acad. Sci. U. S. A. 104, 8143–8148.
17. Hilton, B.J., Anenberg, E., Harrison, T.C., Boyd, J.D., Murphy, T.H., and Tetzlaff, W. (2016). Re-establishment of cortical motor output maps and spontaneous functional recovery via spared dorsolaterally projecting corticospinal neurons after dorsal column spinal cord injury in adult mice. J. Neurosci. 36, 4080–4092.
18. Kumar, S., Black, S.J., Hultman, R., Szabo, S.T., DeMaio, K.D., Du, J., Katz, B.M., Feng, G., Covington, H.E. III, and Dzirasa, K. (2013). Cortical control of affective networks. J. Neurosci. 33, 1116–1129.
19. Ayling, O.G., Harrison, T.C., Boyd, J.D., Goroshkov, A., and Murphy, T.H. (2009). Automated light-based mapping of motor cortex by photoactivation of channelrhodopsin-2 transgenic mice. Nat. Methods 6, 219–224.
20. Hira, R., Honkura, N., Noguchi, J., Maruyama, Y., Augustine, G.J., Kasai, H., and Matsuzaki, M. (2009). Transcranial optogenetic stimulation for functional mapping of the motor cortex. J. Neurosci. Methods 179, 258–263.
21. Massion, J. (1967). The mammalian red nucleus. Physiol. Rev. 47, 383–436.
22. Fanardjian, V.V., Gevorkyan, O.V., Mallina, R.K., Melik-Moussian, A.B., and Meliksetyan, I.B. (2000). Enhanced behavioral recovery from sensorimotor cortex lesions after pyramidotomy in adult rats. Neural Plast. 7, 261–277.
23. Han, Q., Cao, C., Ding, Y., So, K.F., Wu, W., Qu, Y., and Zhou, L. (2015). Plasticity of motor network and function in the absence of corticospinal projection. Exp. Neurol. 267, 194–208.
24. Kadoya, K., Lu, P., Nguyen, K., Lee-Kubli, C., Kumamaru, H., Yao, L., Knackert, J., Poplawski, G., Dulin, J.N., Strobl, H., Takashima, Y., Biane, J., Conner, J., Zhang, S.C., and Tuszynski, M.H. (2016). Spinal cord reconstitution with homologous neural grafts enables robust corticospinal regeneration. Nat. Med. 22, 479–487.
25. Z'Graggen, W.J., Metz, G.A., Kartje, G.L., Thallmair, M., and Schwab, M.E. (1998). Functional recovery and enhanced corticofugal plasticity after unilateral pyramidal tract lesion and blockade of myelin-associated neurite growth inhibitors in adult rats. J. Neurosci. 18, 4744–4757.
26. Liu, N.K., Deng, L.X., Zhang, Y.P., Lu, Q.B., Wang, X.F., Hu, J.G., Oakes, E., Bonventre, J.V., Shields, C.B., and Xu, X.M. (2014). Cytosolic phospholipase A2 protein as a novel therapeutic target for spinal cord injury. Ann. Neurol. 75, 644–658.
27. Basso, D.M., Fisher, L.C., Anderson, A.J., Jakeman, L.B., McTigue, D.M., and Popovich, P.G. (2006). Basso Mouse Scale for locomotion detects differences in recovery after spinal cord injury in five common mouse strains. J. Neurotrauma 23, 635–659.
28. Brittain, J.M., Duarte, D.B., Wilson, S.M., Zhu, W., Ballard, C., Johnson, P.L., Liu, N., Xiong, W., Ripsch, M.S., Wang, Y., Fehrenbacher, J.C., Fitz, S.D., Khanna, M., Park, C.K., Schmutzler, B.S., Cheon, B.M., Due, M.R., Brustovetsky, T., Ashpole, N.M., Hudmon, A., Meroueh, S.O., Hingtgen, C.M., Brustovetsky, N., Ji, R.R., Hurley, J.H., Jin, X., Shekhar, A., Xu, X.M., Oxford, G.S., Vasko, M.R., White, F.A., and Khanna, R. (2011). Suppression of inflammatory and neuropathic pain by uncoupling CRMP-2 from the presynaptic Ca(2)(+) channel complex. Nat. Med. 17, 822–829.
29. Behrmann, D.L., Bresnahan, J.C., Beattie, M.S., and Shah, B.R. (1992). Spinal cord injury produced by consistent mechanical displacement of the cord in rats: behavioral and histologic analysis. J. Neurotrauma 9, 197–217.
30. Liu, N.K., Zhang, Y.P., Han, S., Pei, J., Xu, L.Y., Lu, P.H., Shields, C.B., and Xu, X.M. (2007). Annexin A1 reduces inflammatory reaction and tissue damage through inhibition of phospholipase A2 activation in adult rats following spinal cord injury. J. Neuropathol. Exp. Neurol. 66, 932–943.

31. Xiong, W., and Jin, X. (2012). Optogenetic field potential recording in cortical slices. J. Neurosci. Methods 210, 119–124.
32. Wilson, S.M., Xiong, W., Wang, Y., Ping, X., Head, J.D., Brittain, J.M., Gagare, P.D., Ramachandran, P.V., Jin, X., and Khanna, R. (2012). Prevention of posttraumatic axon sprouting by blocking collapsin response mediator protein 2-mediated neurite outgrowth and tubulin polymerization. Neuroscience 210, 451–466.
33. Joshi, M., and Fehlings, M.G. (2002). Development and characterization of a novel, graded model of clip compressive spinal cord injury in the mouse: part 1. Clip design, behavioral outcomes, and histopathology. J. Neurotrauma 19, 175–190.
34. Zukor, K., Belin, S., Wang, C., Keelan, N., Wang, X., and He, Z. (2013). Short hairpin RNA against PTEN enhances regenerative growth of corticospinal tract axons after spinal cord injury. J. Neurosci. 33, 15350–15361.
35. Joshi, M., and Fehlings, M.G. (2002). Development and characterization of a novel, graded model of clip compressive spinal cord injury in the mouse: part 2. Quantitative neuroanatomical assessment and analysis of the relationships between axonal tracts, residual tissue, and locomotor recovery. J. Neurotrauma 19, 191–203.
36. Li, L., Tasic, B., Micheva, K.D., Ivanov, V.M., Spletter, M.L., Smith, S.J., and Luo, L. (2010). Visualizing the distribution of synapses from individual neurons in the mouse brain. PLoS One 5, e11503.
37. Velazquez, F.N., Caputto, B.L., and Boussin, F.D. (2015). c-Fos importance for brain development. Aging (Albany NY) 7, 1028–1029.
38. Tennant, K.A., Adkins, D.L., Donlan, N.A., Asay, A.L., Thomas, N., Kleim, J.A., and Jones, T.A. (2011). The organization of the forelimb representation of the C57BL/6 mouse motor cortex as defined by intracortical microstimulation and cytoarchitecture. Cereb. Cortex 21, 865–876.
39. Fehlings, M.G., and Tator, C.H. (1995). The relationships among the severity of spinal cord injury, residual neurological function, axon counts, and counts of retrogradely labeled neurons after experimental spinal cord injury. Exp. Neurol. 132, 220–228.
40. McBride, R.L., Feringa, E.R., Garver, M.K., and Williams, J.K., Jr. (1989). Prelabeled red nucleus and sensorimotor cortex neurons of the rat survive 10 and 20 weeks after spinal cord transection. J. Neuropathol. Exp. Neurol. 48, 568–576.
41. Hains, B.C., Black, J.A., and Waxman, S.G. (2003). Primary cortical motor neurons undergo apoptosis after axotomizing spinal cord injury. J. Comp. Neurol. 462, 328–341.
42. Akemann, W., Zhong, Y.M., Ichinohe, N., Rockland, K.S., and Knopfel, T. (2004). Transgenic mice expressing a fluorescent in vivo label in a distinct subpopulation of neocortical layer 5 pyramidal cells. J. Comp. Neurol. 480, 72–88.
43. Novikova, L.N., Novikov, L.N., and Kellerth, J.O. (2000). Survival effects of BDNF and NT-3 on axotomized rubrospinal neurons depend on the temporal pattern of neurotrophin administration. Eur. J. Neurosci. 12, 776–780.
44. Wise, S.P., and Jones, E.G. (1977). Cells of origin and terminal distribution of descending projections of the rat somatic sensory cortex. J. Comp. Neurol. 175, 129–157.
45. Carmel, J.B., and Martin, J.H. (2014). Motor cortex electrical stimulation augments sprouting of the corticospinal tract and promotes recovery of motor function. Front. Integr. Neurosci. 8, 51.
46. Brown, L.T. (1974). Corticorubral projections in the rat. J. Comp. Neurol. 154, 149–167.
47. Flumerfelt, B.A. (1980). An ultrastructural investigation of afferent connections of the red nucleus in the rat. J. Anat. 131, 621–633.
48. King, J.S., Martin, G.F., and Conner, J.B. (1972). A light and electron microscopic study of corticorubral projections in the opossum, Didelphis marsupialis virginiana. Brain Res. 38, 251–265.
49. Leclerc, N., Beesley, P.W., Brown, I., Colonnier, M., Gurd, J.W., Paladino, T., and Hawkes, R. (1989). Synaptophysin expression during synaptogenesis in the rat cerebellar cortex. J. Comp. Neurol. 280, 197–212.
50. Wiedenmann, B., and Franke, W.W. (1985). Identification and localization of synaptophysin, an integral membrane glycoprotein of Mr 38,000 characteristic of presynaptic vesicles. Cell 41, 1017–1028.
51. Bergmann, M., Post, A., Rittel, I., Bechmann, I., and Nitsch, R. (1997). Expression of synaptophysin in sprouting neurons after entorhinal lesion in the rat. Exp. Brain Res. 117, 80–86.
52. Tsukahara, N., Fujito, Y., Oda, Y., and Maeda, J. (1982). Formation of functional synapses in the adult cat red nucleus from the cerebrum following cross-innervating of forelimb flexor and extensor nerves. I. Appearance of new synaptic potentials. Exp. Brain Res. 45, 1–12.
53. Andrews, E.M., Tsai, S.Y., Johnson, S.C., Farrer, J.R., Wagner, J.P., Kopen, G.C., and Kartje, G.L. (2008). Human adult bone marrow-derived somatic cell therapy results in functional recovery and axonal plasticity following stroke in the rat. Exp. Neurol. 211, 588–592.
54. Lawrence, D.G., and Kuypers, H.G. (1968). The functional organization of the motor system in the monkey. I. The effects of bilateral pyramidal lesions. Brain 91, 1–14.
55. Lawrence, D.G., and Kuypers, H.G. (1968). The functional organization of the motor system in the monkey. II. The effects of lesions of the descending brain-stem pathways. Brain 91, 15–36.

Address correspondence to:
Xiaoming Jin, PhD
Stark Neurosciences Research Institute
Indiana University School of Medicine
320 West 15th Street
NB 500C
Indianapolis, IN 46202

E-mail: xijin@iupui.edu